

## Article

# Photodetector-Based Material from a Highly Sensitive Free-Standing Graphene Oxide/Polypyrrole Nanocomposite

Amira Ben Gouider Trabelsi <sup>1</sup>, Asmaa M. Elsayed <sup>2,3</sup>, Fatemah. H. Alkallas <sup>1,\*</sup>, Salem AlFaify <sup>4</sup>, Mohd. Shkir <sup>4,5</sup>, Tahani A. Alrebdi <sup>1</sup>, Kholoud S. Almgren <sup>1</sup>, Feodor V. Kusmatsev <sup>6</sup> and Mohamed Rabia <sup>2,7,\*</sup>

<sup>1</sup> Department of Physics, College of Science, Princess Nourah Bint Abdulrahman University, P.O. Box 84428, Riyadh 11671, Saudi Arabia; aatrabelsi@pnu.edu.sa (A.B.G.T.)

<sup>2</sup> Nanophotonics and Applications Lab, Physics Department, Faculty of Science, Beni-Suef University, Beni-Suef 62514, Egypt

<sup>3</sup> TH-PPM Group, Physics Department, Faculty of Science, Beni-Suef University, Beni-Suef 62514, Egypt

<sup>4</sup> Advanced Functional Materials & Optoelectronic Laboratory (AFMOL), Department of Physics, Faculty of Science, King Khalid University, Abha 61413, Saudi Arabia

<sup>5</sup> Department of Chemistry and University Centre for Research & Development, Chandigarh University, Mohali 140413, Punjab, India

<sup>6</sup> Department of Physics, Khalifa University of Science and Technology, Abu Dhabi 127788, United Arab Emirates

<sup>7</sup> Nanomaterials Science Research Laboratory, Chemistry Department, Faculty of Science, Beni-Suef University, Beni-Suef 62514, Egypt

\* Correspondence: fhalkallas@pnu.edu.sa (F.H.A.); mohamedchem@science.bsu.edu.eg (M.R.)

**Abstract:** This paper describes the establishment of free-standing rolled graphene oxide (roll-GO) and polypyrrole (Ppy) using a modified Hummer method and oxidative polymerization. Then, a photodetector was created by removing a thin film of the free-standing rolled graphene oxide from a filter paper and attaching it to a tape. The chemical structure of the roll-GO was confirmed using XRD and FTIR analysis, while SEM and TEM showed that it was rolled in nature. The material had a small bandgap of 2.4 eV and a high current density in light conditions. The photodetector responded well to monochromatic light, with  $J_{ph}$  values changing from 0.027 to 0.019 mA/cm<sup>2</sup> as the light wavelengths decreased from 340 to 730 nm. The photoresponsivity (R) and detectivity (D) values were high, at 340 nm (0.27 mA/W and  $6.0 \times 10^7$  Jones, respectively) and at 730 nm (0.19 and  $4.25 \times 10^7$  Jones, respectively). The addition of Ppy improved these parameters, with the Ppy/roll-GO/tape photoelectrode showing excellent R and D values of 0.33 mA/W and  $7.34 \times 10^7$  Jones, respectively. Furthermore, the production of a photocurrent at  $V = 0$  indicated that the Ppy/roll-GO layer could be used for solar cell applications. Overall, the results suggest that the prepared free-standing Ppy/roll-GO/tape photodetector has high potential for use in the optical region between 340 and 730 nm and may be suitable for industrial applications.

**Keywords:** free-standing graphene oxide; polypyrrole; Hummer method; oxidative polymerization; current density; monochromatic light; photoresponsivity; photoelectrode; photocurrent; solar cell applications



**Citation:** Ben Gouider Trabelsi, A.; M. Elsayed, A.; Alkallas, F.H.; AlFaify, S.; Shkir, M.; Alrebdi, T.A.; Almgren, K.S.; Kusmatsev, F.V.; Rabia, M. Photodetector-Based Material from a Highly Sensitive Free-Standing Graphene Oxide/Polypyrrole Nanocomposite. *Coatings* **2023**, *13*, 1198. <https://doi.org/10.3390/coatings13071198>

Academic Editor: Cristian Vacacela Gomez

Received: 3 May 2023

Revised: 21 June 2023

Accepted: 28 June 2023

Published: 4 July 2023



**Copyright:** © 2023 by the authors. Licensee MDPI, Basel, Switzerland. This article is an open access article distributed under the terms and conditions of the Creative Commons Attribution (CC BY) license (<https://creativecommons.org/licenses/by/4.0/>).

## 1. Introduction

Photodetectors have become crucial optoelectronic devices for various applications, including communication, lighting, and renewable energy. They are highly efficient in converting light into electrical signals [1–4]. These devices work by absorbing photons, the particles of light, and using their energy to generate an electrical current. The resulting current can then be measured and used for detecting light, measuring light intensity, or capturing images. Common types of photodetectors include photoresistors, photodiodes, and phototransistors. While materials such as silicon, III-V semiconductors, and germanium have traditionally been used for photodetectors, they still face limitations, such as a

limited direct light detection capability. This has led researchers to explore new materials for photodetectors [5–8].

Graphene, a unique two-dimensional carbon allotrope composed of a single layer of carbon atoms arranged in honeycomb lattices, has shown promise as a photodetector material. Its exceptional optical properties, such as its high absorbance of incident light (around 2.3%) despite its small thickness [9–11] and gapless nature, which allows for the generation of charge carriers over a wide optical range, make it suitable for wide-ranging optical domains including visible, near-infrared, and mid-infrared. Graphene-based photodetectors are different from semiconductor photodetectors in that incident light can reach the detection layer without being absorbed by a substrate or semiconducting layer. This is due to the fact that the detection layer is made of graphene placed on the substrate, which ensures better detection over a large optical range.

A photodetector's sensitivity is a critical factor in determining its efficiency, as it is highly dependent on the device's ability to accept incident photons. Once a photon is absorbed, the surface of the photodetector is activated, leading to the generation of electrons and the production of a current density ( $J_{ph}$ ). Previous research has shown that the  $J_{ph}$  value can be increased by increasing the number of active sites in the photodetector material. Inorganic materials in the sheet or rolled form have shown promise in achieving higher sensitivity. For example, Wang et al. [12] reported a photocurrent ( $J_{ph}$ ) value of 20  $\mu\text{A}$  at +5 V, while Bai et al. [13] achieved a higher  $J_{ph}$  value of 107  $\mu\text{A}$ . Other studies have focused on different nanomaterial systems, such as Al-CdS [14] and CdS-ZnO [15]. In these cases, the  $J_{ph}$  values were found to be significantly lower, with values of  $10^{-5}$  and  $10^{-11}$  A, respectively. These low values suggest that these materials have a limited response and efficiency when generating photocurrents in response to incident photons.

Conducting polymers are often used to enhance the efficiency of photodetectors due to their numerous technical benefits, such as their high optical absorbance and suitable bandgap properties. In addition, these materials are easy to synthesize and can be prepared in large quantities, making them a good choice for light-sensing applications. Polypyrrole is one of the promising conducting polymers for optoelectronics due to its semiconductor properties. Its small particle size makes it ideal for combination with carbon materials to develop new composites, providing great control over the material's optical and electrical properties [16,17]. However, previous studies have shown that the composite's efficiency is low, and the synthesis techniques are expensive.

In this study, we prepared a free-standing Ppy/roll-GO/tape photodetector. The device has a large surface area, making it highly sensitive to light in the UV, Vis, and NIR regions. We analyzed the material's optical, structural, and morphological properties using SEM, TEM, FTIR, and optical measurements. We also studied the photodetector's electrochemical properties using a CHI660E PowerStation. We examined the effects of dark and light, as well as monochromatic light wavelengths ranging from 340 to 730 nm. The photocurrent production of the device illustrates its potential for solar cell applications. Finally, we determined the photodetector's efficiency by calculating the R and D values, which showed promising results for future improvements in photodetection technology.

## 2. Materials and Methods

### 2.1. Roll-GO Material Synthesis

The GO material used in this study was synthesized using a modified Hummer's method. In this method, 1.0 g of graphite powder was suspended in a mixture of highly concentrated  $\text{H}_2\text{SO}_4$  (99.9%) and  $\text{H}_3\text{PO}_4$  (99.9%) under stirring conditions. Then,  $\text{KMnO}_4$  was added to the mixture to separate the graphite layers. This process was maintained for one day under stirring conditions. The excess  $\text{KMnO}_4$  was removed by adding 8 mL of high-concentration  $\text{H}_2\text{O}_2$  on the second day, resulting in a faint brownish-yellow color indicating the formation of GO materials (11 mg/mL). The GO materials were kept in the suspended solution for 10 days to form the roll-GO used in the photodetector.

## 2.2. Free-Standing Roll-GO/Tape Synthesis

The free-standing roll-GO/tape was developed through the filtration of the roll-GO materials (11 mg/mL) using a Whatman filter paper (Sigma-Aldrich, St. Louis, MO, USA), followed by well washing of the precipitate using distilled water. The filter paper with the precipitate was then dried for three days at room temperature. The resulting free-standing Roll-Go film was then removed from the filter paper and attached to a tape, producing a flexible, free-standing roll-GO/tape.

## 2.3. Free-Standing Ppy/Roll-GO/Tape Synthesis

In this study, a free-standing Ppy/roll-GO material was created by coating the roll-GO/tape with Ppy. This was achieved through in situ polymerization of the Ppy over the roll-GO/tape. Pyrrole was dissolved in 0.5 M HCl, and  $K_2S_2O_8$  was added to the monomer to coat the roll-GO/tape with a Ppy film.

## 2.4. Characterization Process

The chemical structure of the sample was confirmed using a Jasco 340 spectrophotometer for Fourier transform infrared (FTIR) spectroscopy and a PANalytical Pro X-ray diffractometer (XRD) (Malvern Panalytical, Malvern, UK). Morphological analysis was conducted using the JEOL JEM-2100 TEM (JEOL, Tokyo, Japan) and ZEISS (Gemini) SEM models (ZEISS, Jena, Germany) for transmitted and scanning electron microscopes, respectively. The optical properties were determined using a UV/Vis spectrophotometer from Birkin Elmer, Waltham, MA, USA.

## 2.5. The Electrochemical Testing of the Photodetector and Solar Cell

The electrochemical properties of the free-standing roll-GO/tape and Ppy/roll-GO/tape were studied using an electrochemical workstation (CHI608E) (CH Instruments, Inc., Bee Cave, TX, USA), and an Ag paste was added to each side of the photodetector, for which the distance between the two sides was 1 cm. To measure the photo response of the electrode, a 400 W metal halide lamp was used, and the effects of light and dark conditions, as well as monochromatic wavelengths, were studied. These measurements were performed at 25 °C with normal atmospheric pressure. The generation of a photocurrent indicated the validity of this construction for solar cell applications. Photoresponsivity and detectivity were used to assess the efficiency of the photoelectrode. Figure 1 illustrates the experimental setup developed for electrochemical testing.

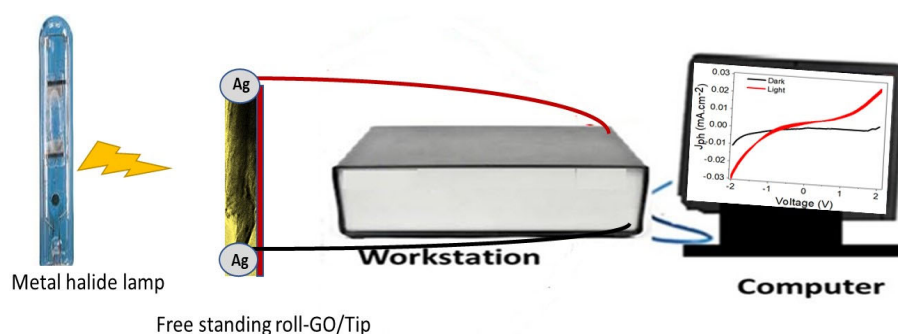


**Figure 1.** The electrochemical testing of the free-standing roll-GO/tape with/without the Ppy film as a photodetector or solar cell using the electrochemical workstation.

## 3. Results and Discussion

### 3.1. Characterization Process

The morphology of the free-standing roll-GO material was examined using SEM and TEM microscopies (see Figure 2a,b). The theoretical simulation of the roll-GO material also performed (see Figure 2c,d). Furthermore, SEM images of the Ppy at various magnifications are represented in Figure 2e,f.

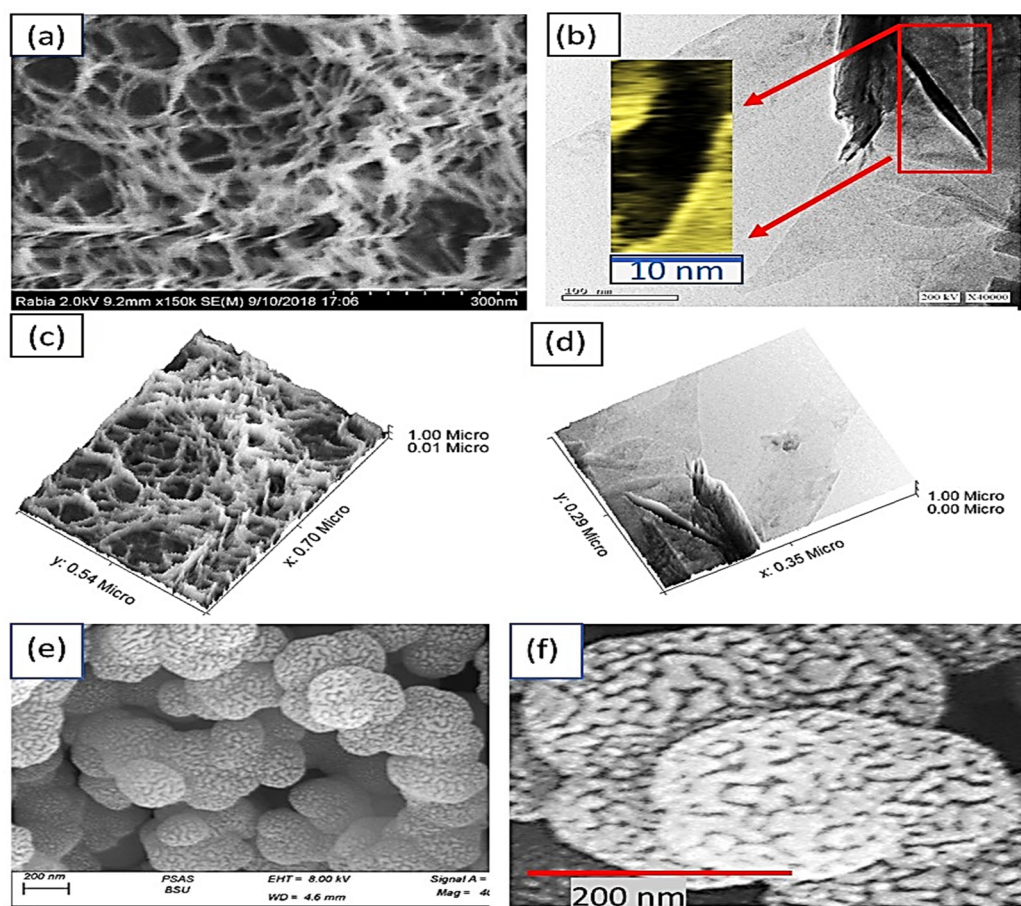


**Figure 2.** (a) SEM. (b) TEM. Here, (c) provides a theoretical simulation that confirms the 2D rolled structure of the roll-GO, showing both face and cross-sectional views. Additionally, Figure 2d shows the same behavior of the roll-GP, revealing the formation of a tube with an approximate diameter of 10 nm. (e,f) SEM of Ppy at different magnifications.

The scanning electron microscopy (SEM) and transmission electron microscopy (TEM) images presented in this study provide a clear visualization of the unique morphology of the free-standing roll-GO/tape material [18,19]. The SEM images reveal a highly rolled 2D sheet with a diameter of 10 nm and a length of 300 nm, providing a large surface area and increased porosity that enhances the material's electrochemical properties. The theoretical simulation presented in Figure 2c confirms the 2D rolled structure of the roll-GO and shows both the face and cross-sectional views. Moreover, the SEM images confirm the formation of a 2D free-standing roll-GO network, which efficiently captures the light passing through the pores of the roll-GO, further enhancing its photoelectrochemical properties.

Furthermore, the SEM images in Figure 2e,f clearly show the formation of porous spherical Ppy particles during the polymerization reaction [20–22]. These particles are composed of smaller agglomerated particles forming a new, larger, spherical structure. This unique morphology was expected to have a significant impact on the properties of the composite material, potentially enhancing its performance in various applications.

Overall, the SEM and TEM images provide a clear visualization of the unique morphology of the free-standing roll-GO/tape material and the Ppy particles formed during the polymerization reaction. The high porosity and surface area of the roll-GO network and the unique morphology of the Ppy particles are expected to have significant impacts on the properties of the composite material, making it a promising candidate for various applications.

The FTIR measurements confirm the presence of functional groups in the free-standing roll-GO structure (see, Figure 3a). The O-H and C-O epoxide functional groups are observed

at 3440 and 1174  $\text{cm}^{-1}$ , respectively. In addition, the functional groups of Ppy are clearly identified (see Figure 3b). The functional groups located at 1708, 1630, 1532, and 1450  $\text{cm}^{-1}$  correspond to the Ppy ring, while the C=N and C-N functional groups are located at 1300 and 1160  $\text{cm}^{-1}$ , respectively [23]. The out-of-plane functional group at 670  $\text{cm}^{-1}$  is also confirmed.

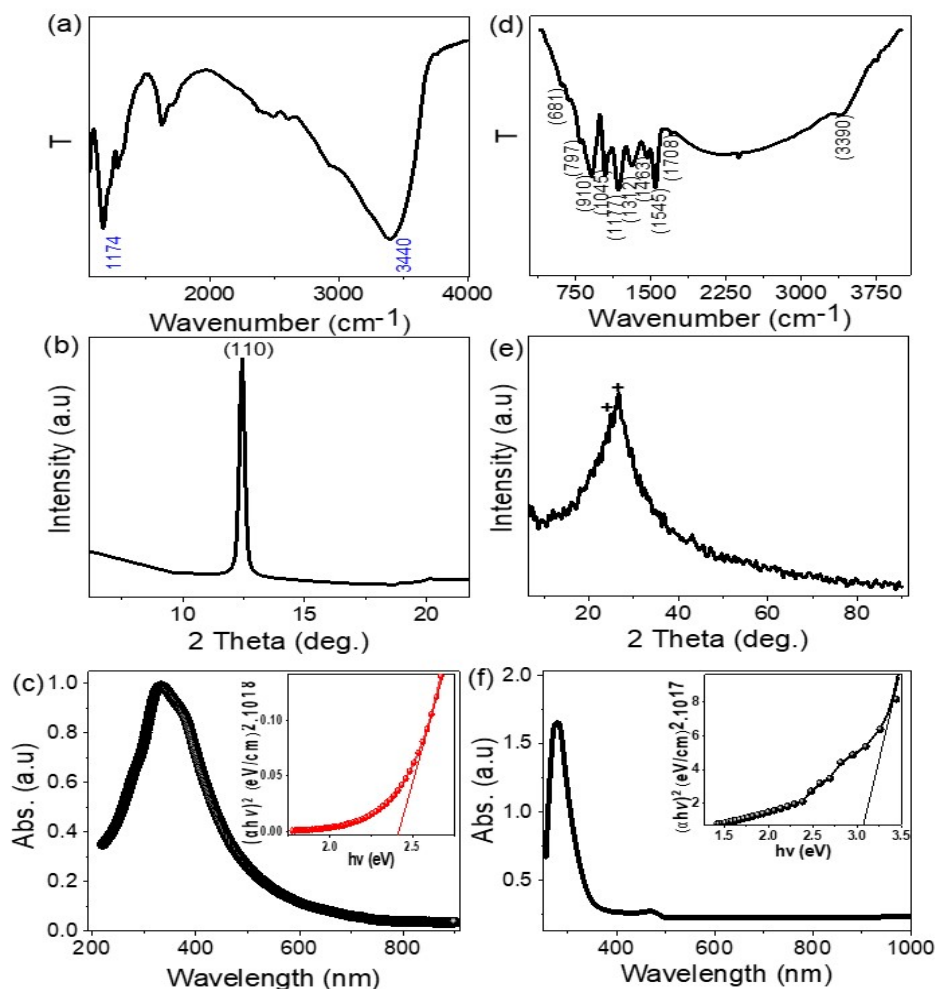


**Figure 3.** (a,d) FTIR, (b,e) XRD, and (c,f) absorbance values for the roll-GO and Ppy nanomaterials (inserting bandgap drawn from the Tauc equation), respectively.

The XRD analysis demonstrates a sharp and distinct peak for the roll-GO material at  $2\theta = 11^\circ$  that corresponds to the (110) growth direction (see Figure 3c), in which the formation of a single peak indicates the single phase of this nanomaterial. The high intensity of this peak indicates the high crystallinity of the prepared roll-GO materials [24]. The crystalline size ( $D$ ) of the roll-GO was determined by analyzing the high peak using the Scherrer equation, which relates the size to the full-width half maximum ( $W$ ) of the peak, the XRD wavelength ( $\lambda$ ), and the angle of diffraction ( $\theta$ ). According to the Scherrer equation,  $D$  can be calculated as  $D = 0.9\lambda / (W \cdot \cos \theta)$  [25]. By applying this equation, the crystalline size of the roll-GO was determined to be 41 nm.

For the Ppy porous spherical nanomaterial, the presence of a broad peak followed by two small semi-sharp peaks at  $2\theta = 24.7^\circ$  and  $26.4^\circ$  in the XRD pattern indicates the amorphous nature of the Ppy (see, Figure 3d).

The optical absorbance of the prepared roll-GO material is shown in Figure 3e. The absorbance extends from the UV to the visible region, with a broad band. This is related to the electronic transitions from lower to higher energy levels under photon excitation and is also related to the material's bandgap [26–28]. Figure 3f represents the optical absorbance

of the Ppy, which exhibits a high absorbance behavior in the UV region due to electron transitions to higher energy levels. The bandgap ( $E_g$ ) of the materials can be calculated using the Tauc equation (Equations (1) and (2)), given by:

$$\alpha h\nu = A(h\nu - E_g)^{1/2} \tag{1}$$

$$\alpha = \left(\frac{2303}{d}\right)A \tag{2}$$

where  $\alpha$ ,  $A$ ,  $h$ , and  $\nu$  are assigned to the absorption coefficient, absorbance, Planck constant, and the frequency, respectively. The bandgap energy is an important parameter that determines the material’s electronic properties and its ability to absorb light at different wavelengths. In this case, the roll-GO material demonstrates a bandgap of 2.41 eV, while the Ppy material has a bandgap of 2.51 eV. These values indicate that both materials have high light absorbance in the UV, visible, and near-IR regions.

### 3.2. Electrochemical Study

The photodetection performance of the free-standing roll-GO/Tape material was evaluated using an electrochemical workstation (CHI608E) with silver paste coated on each side of the photodetector to enable connection. The voltage was scanned from  $-2.0$  to  $+2.0$  V at a rate of 100 mV, and the photodetection capability was investigated under dark and light conditions and at different monochromatic wavelengths. As shown in Figure 4, the free-standing roll-GO/Tape photodetector demonstrated a significant response to light, with  $J_{ph}$  values increasing from 0.006 to 0.027 mA/cm<sup>2</sup> in dark and light conditions, respectively, at 2.0 V. This high response to light confirms the sensitivity of the prepared photodetector, with incident photons exciting electrons under level splitting and hot electrons being collected on the conducting band of the roll-GO material, resulting in an increase in the  $J_{ph}$  values.

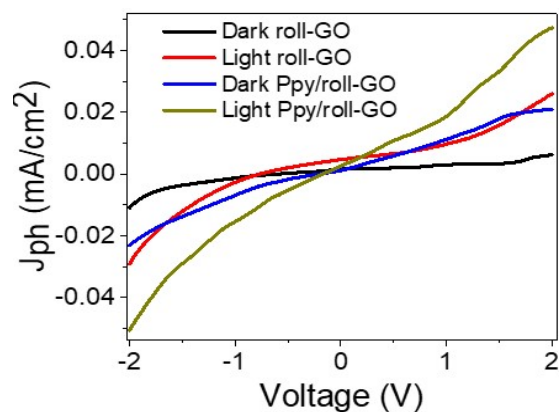


**Figure 4.** The effects of dark and light conditions on the responsivity of the prepared photodetector or solar cell using electrochemical measurements in the presence or absence of Ppy-film-coated roll-GO/Tape.

The semiconductive nature of the GO material and the effect of oxidizing gases in the ambient air on the electrode surface contribute to the small and negligible current density in the dark ( $J_0$ ) [25]. Furthermore, the photodetector’s response to photons in a wide range of optical regions, from UV to Vis, is confirmed by these findings [27]. The addition of Ppy to the roll-GO resulted in a significant increase in the  $J_{ph}$  values, reaching up to 0.05 mA/cm<sup>2</sup>. This increase can be attributed to the rise of electron clouds in the conducting band, leading to a substantial increase in the  $J_{ph}$  values. This phenomenon of generating a large photocurrent at  $V = 0$  makes this device promising for solar cell applications, with  $J_{ph} = J_{sc}$  reaching  $2.0 \mu A \cdot cm^{-2}$ .

The photo response of the free-standing roll-GO material was examined at monochromatic wavelengths in the range of 340 to 730 nm using an electrochemical workstation (Figure 5). The results showed that the  $J_{ph}$  values varied from 0.027 to 0.019 mA/cm<sup>2</sup> with an increase in the monochromatic wavelength light from 340 to 730 nm, respectively. This variation could be attributed to the difference in light frequency, whereas the frequency increased, electrons transited from the valence to the conduction band, resulting in an increase in  $J_{ph}$ . Despite the variation in the  $J_{ph}$  values from the UV to IR regions, they remained significant, indicating the photodetector's ability to detect light in the UV to near-IR range.

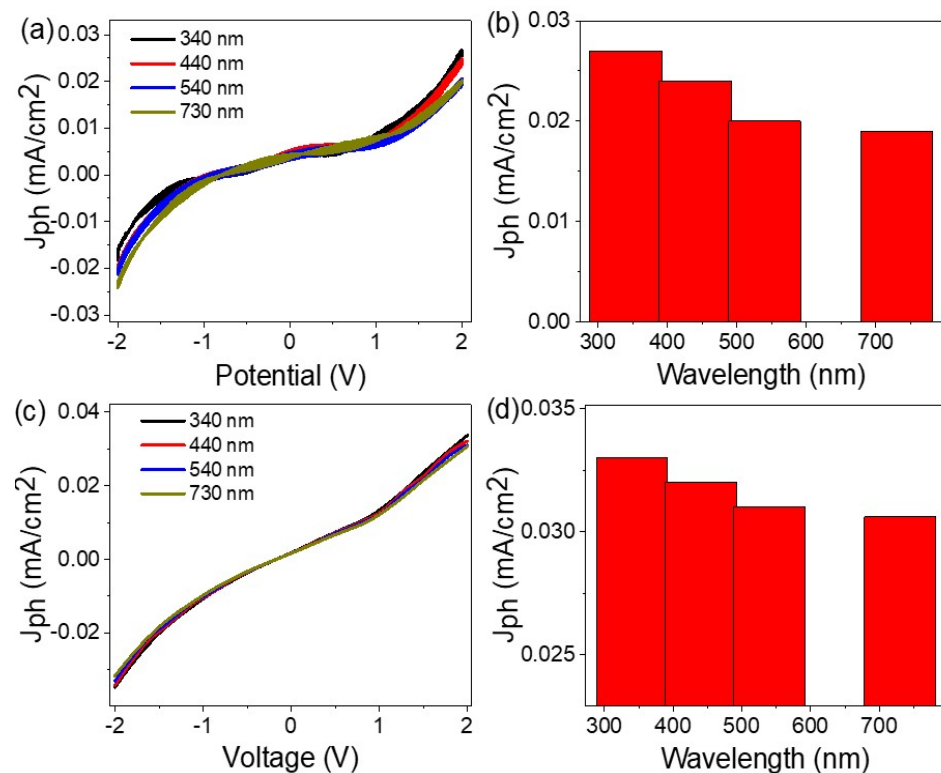


**Figure 5.** (a,b) The effects of light wavelengths (340, 440, 540, and 730 nm) on the prepared free-standing roll-GO/tape photodetector and (c,d) effect after the incorporation of Ppy.

Furthermore, the addition of the Ppy nanomaterial to the roll-GO material in the Ppy/roll-GO/tape photodetector enhanced the photoresponsivity at different wavelengths, as reflected in the  $J_{ph}$  values. At 340 nm, the  $J_{ph}$  values increased to 0.033 mA/cm<sup>2</sup>, indicating an enhancement at 2.0 V. These properties make the prepared photodetector promising for various industrial applications, such as use in high-technology devices like cameras or space rockets [29,30].

To determine the number of photons, a metal halide lamp of 100 mW·cm<sup>-2</sup> was used. Equation (3) can be used to determine such a photon's number [31], where ( $\lambda$ ) is the light wavelength, ( $c$ ) is the speed, ( $h$ ) is the Planck constant, and using light intensity ( $P$ ). The calculated number of photons was found to be  $8 \times 10^{21}$  photons/s, which is almost equal to the number of electrons collected on the surface of the roll-GO materials, as indicated by the  $J_{ph}$  values.

$$N = \lambda P / hc \quad (3)$$

The photoresponsivity ( $R$ ) of the prepared roll-GO materials was determined using Equation (4), where  $J_{ph}$  and  $J_0$  represent the current densities in light and dark conditions, respectively, and ( $P$ ) is the light power. Furthermore, the detectivity ( $D$ ) was also deter-

mined using Equation (5) [32]. Indeed,  $D$  depends on the  $R$  values, as well as the electron charge ( $e$ ) and area of the photodetector ( $A$ ).

$$R = \frac{J_{ph} - J_o}{P} \quad (4)$$

$$D = R \sqrt{A / 2 e J_o} \quad (5)$$

The  $R$  values of the prepared roll-GO materials decrease as the monochromatic wavelengths increase from 340 to 730 nm. At 340 nm, the  $R$  value is  $0.27 \text{ mA/W}^1$ , while at 730 nm, it is  $0.19 \text{ mA/W}^1$  (see Figure 6a,b). Similarly, the detectivity ( $D$ ) values of the photodetector decrease from  $6.0 \times 10^7$  to  $4.25 \times 10^7$  Jones as the monochromatic wavelengths increase. However, the incorporation of Ppy into the structure leads to significant improvements in both the  $R$  and  $D$  values. The Ppy/roll-GO/tape photoelectrode exhibits excellent  $R$  and  $D$  values of  $0.33 \text{ mA/W}^1$  and  $7.34 \times 10^7$  Jones, respectively (see Figure 6c,d).

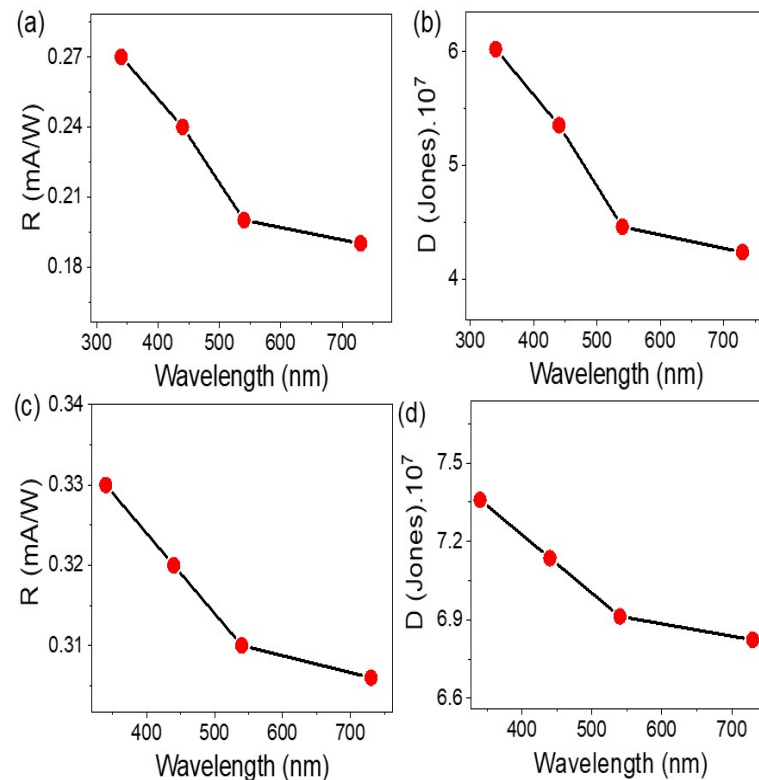


**Figure 6.** (a)  $R$  and (b)  $D$  values for the prepared free-standing roll-GO/tape photodetector, while (c,d) represent the corresponding  $R$  and  $D$  values for the Ppy/roll-GO/tape photodetector.

The obtained results demonstrate the good photodetector properties of the Ppy/roll-GO/tape photodetector compared to previous studies, as summarized in Table 1. The photodetector shows higher photoresponsivity and detectivity in a wider range of wavelengths, from UV to near-IR, which is attributed to the semiconductive nature of the GO material and the enhancements provided through the Ppy nanomaterial. Additionally, the photodetector has a low dark current density, indicating its ability to operate in low-light conditions. These properties make the photodetector a promising candidate for industrial applications such as high-tech cameras or space rockets, for which a high sensitivity and low cost are desired. Thus, the production of a photocurrent at  $V = 0$  indicates the potential of these two contact layers as a solar cell.

**Table 1.** The R performance of the free-standing roll-GO/tape photodetector in comparison with the literature.

Photoelectrode	Wavelength (nm)	Bandgap (eV)	Bais (V)	R (mA/W)
GeSe/CdS Heterojunctions [33]	White light	1.4	0.8	0.1
ZnCdSe/ZnCdMgSe [34]	White light	-	4	0.1
Polyaniline/MgZnO [35]	250	3.3	5	0.1
Graphene/GaN [36]	365	-	7	$3 \times 10^{-3}$
ZnO-CuO [37]	405	3.34	1	$3 \times 10^{-3}$
CuO/Si Nanowire [38]	405	1.35	0.2	$3.8 \times 10^{-3}$
Graphene/P3HT [39]	325	-	1	NA
GO/Cu <sub>2</sub> O [40]	300	2	2	$0.5 \times 10^{-3}$
ZnO/RGO [41]	350	3.47	5	$1.3 \times 10^{-3}$
2,1,3-Benzothiadiazole [42]	734	-	0	NA
Polyvinylpyrrolidone/CsPbBr <sub>3</sub> [43]	500	2.3	2	NA
CuO Nanowires [12]	390	1.2	5	-
ZnO/Cu <sub>2</sub> O [13]	350	2.4	2	$4 \times 10^{-3}$
TiO <sub>2</sub> /NiO [44]	350	2.85	0	$0.4 \times 10^{-3}$
TiN/TiO <sub>2</sub> [45]	550	2.6	5	-
Se/TiO <sub>2</sub> [46]	450	1.62	1	$5 \times 10^{-3}$
TiO <sub>2</sub> -PANI [47]	320	-	0	$3 \times 10^{-3}$
Free-sStanding Roll-GO/Tape (this work)	440	2.41	2	0.24

NA: without mentioned value.

Overall, the results demonstrate the high sensitivity and promising performance of the free-standing roll-GO/tape photodetector in detecting light in a wide range of optical regions. This device has potential for applications in various fields, including simple light sensors in everyday devices like smartphones and automatic lights, as well as more complex uses in fields such as astronomy, communications, and medical imaging.

#### 4. Conclusions

In this study, we developed a low-cost, free-standing roll-GO/tape photodetector that can detect light in the far optical region from UV to IR. We used various characterization techniques, including FTIR, XRD, TM, SEM, and a spectrophotometer, to analyze the chemical, morphological, and optical properties of the photodetector. The prepared GO rolled tubes had a diameter of 10 nm and showed promising optical properties, with a small band gap value of 2.41 eV. We evaluated the photodetector's efficiency under different parameters, including light and dark conditions and monochromatic light wavelengths, using  $J_{ph}$  values. The  $J_{ph}$  values increased from 0.006 to 0.027 mA/cm<sup>2</sup> under dark and light conditions, respectively, while the R and D values decreased from 0.027 to 0.019 mA/W<sup>1</sup> and from  $6.0 \times 10^7$  to  $4.25 \times 10^7$  Jones, respectively, with decreasing light wavelengths from 340 to 730 nm. By incorporating Ppy into the structure, we significantly improved the R and D values, which increased to 0.33 mA/W<sup>1</sup> and  $7.34 \times 10^7$  Jones, respectively. The free-standing Ppy/roll-GO/tape photodetector has excellent optical and economical properties, making it suitable for light detection in a wide optical region, from UV to IR, and for industrial applications. The device is also valuable for solar cell applications, as its  $J_{ph} = J_{Sc}$  reached 2.0  $\mu$ A/cm<sup>2</sup> at V = 0. Therefore, we believe that our photodetectors have a wide range of potential applications, from simple light sensors in everyday devices like smartphones and automatic lights to more complex uses in fields such as astronomy, communications, and medical imaging.

**Author Contributions:** Conceptualization, A.B.G.T., A.M.E., F.H.A., F.V.K. and M.R.; methodology, A.B.G.T., A.M.E., F.H.A., S.A., M.S., T.A.A., K.S.A., F.V.K. and M.R.; formal analysis, A.B.G.T., A.M.E., F.H.A., S.A., M.S., T.A.A., K.S.A., F.V.K. and M.R.; investigation, A.B.G.T., A.M.E., F.H.A., F.V.K. and M.R.; resources, S.A., M.S., T.A.A., K.S.A. and F.V.K.; writing—original draft preparation, A.B.G.T., A.M.E., F.H.A., F.V.K. and M.R.; writing—review and editing, F.H.A., A.M.E., A.B.G.T., S.A., M.S.,

T.A.A., K.S.A., F.V.K. and M.R.; supervision, A.B.G.T., A.M.E., F.H.A., F.V.K. and M.R.; project administration, S.A., M.S., T.A.A., K.S.A. and F.V.K.; funding acquisition, F.H.A. and A.B.G.T. All authors have read and agreed to the published version of the manuscript.

**Funding:** This work was funded by the Deanship of Scientific Research at Princess Nourah bint Abdulrahman University through the Research Groups Program (Grant No. RGP-1442-0034).

**Institutional Review Board Statement:** Not applicable.

**Informed Consent Statement:** Not applicable.

**Data Availability Statement:** Not applicable.

**Acknowledgments:** The authors express their gratitude to the Deanship of Scientific Research at Princess Nourah bint Abdulrahman University, through the Research Groups Program Grant no. (RGP-1442-0034).

**Conflicts of Interest:** The authors declare no conflict of interest.

## References

- Lopez, G.; Santamaria, L.; Lemonidou, A.; Zhang, S.; Wu, C.; Sipra, A.T.; Gao, N. Hydrogen generation from biomass by pyrolysis. *Nat. Rev. Methods Prim.* **2022**, *2*, 20. [[CrossRef](#)]
- Hu, Z.-Y.; Zhang, Y.-L.; Pan, C.; Dou, J.-Y.; Li, Z.-Z.; Tian, Z.-N.; Mao, J.-W.; Chen, Q.-D.; Sun, H.-B. Miniature optoelectronic compound eye camera. *Nat. Commun.* **2022**, *13*, 5634. [[CrossRef](#)] [[PubMed](#)]
- Wu, S.; Chen, Y.; Wang, X.; Jiao, H.; Zhao, Q.; Huang, X.; Tai, X.; Zhou, Y.; Chen, H.; Wang, X.; et al. Ultra-sensitive polarization-resolved black phosphorus homojunction photodetector defined by ferroelectric domains. *Nat. Commun.* **2022**, *13*, 3198. [[CrossRef](#)] [[PubMed](#)]
- Liu, Y.; Liu, C.-H.; Debnath, T.; Wang, Y.; Pohl, D.; Besteiro, L.V.; Meira, D.M.; Huang, S.; Yang, F.; Rellinghaus, B.; et al. Silver nanoparticle enhanced metal-organic matrix with interface-engineering for efficient photocatalytic hydrogen evolution. *Nat. Commun.* **2023**, *14*, 541. [[CrossRef](#)] [[PubMed](#)]
- Abdelazeez, A.A.A.; Trabelsi, A.B.G.; Alkallas, F.; Rabia, M. Successful 2D MoS<sub>2</sub> nanosheets synthesis with SnSe grid-like nanoparticles: Photoelectrochemical hydrogen generation and solar cell applications. *Sol. Energy* **2022**, *248*, 251–259. [[CrossRef](#)]
- Alkallas, F.H.; Elsayed, A.M.; Trabelsi, A.B.G.; AlFaify, S.; Shkir, M.; Alrebdi, T.A.; Almugren, K.S.; Kusmatsev, F.V.; Rabia, M. Impact of Rolled Graphene Oxide Grown on Polyaniline for Photodetection: Future Challenging Opto-Device. *Coatings* **2023**, *13*, 437. [[CrossRef](#)]
- Elsayed, A.M.; Alkallas, F.H.; Trabelsi, A.B.G.; AlFaify, S.; Shkir, M.; Alrebdi, T.A.; Almugren, K.S.; Kusmatsev, F.V.; Rabia, M. Photodetection Enhancement via Graphene Oxide Deposition on Poly 3-Methyl Aniline. *Micromachines* **2023**, *14*, 606. [[CrossRef](#)]
- Alkallas, F.H.; Trabelsi, A.B.G.; Alrebdi, T.A.; Ahmed, A.M.; Rabia, M. Development of a Highly Efficient Optoelectronic Device Based on CuFeO<sub>2</sub>/CuO/Cu Composite Nanomaterials. *Materials* **2022**, *15*, 6857. [[CrossRef](#)]
- Mohanadas, D.; Abdah, M.A.A.M.; Azman, N.H.N.; Ravoof, T.B.S.A.; Sulaiman, Y. Facile synthesis of PEDOT-rGO/HKUST-1 for high performance symmetrical supercapacitor device. *Sci. Rep.* **2021**, *11*, 11747. [[CrossRef](#)]
- Kulandaivalu, S.; Suhaimi, N.; Sulaiman, Y. Unveiling high specific energy supercapacitor from layer-by-layer assembled polypyrrole/graphene oxide | polypyrrole/manganese oxide electrode material. *Sci. Rep.* **2019**, *9*, 4884. [[CrossRef](#)]
- Yoshioka, K.; Wakamura, T.; Hashisaka, M.; Watanabe, K.; Taniguchi, T.; Kumada, N. Ultrafast intrinsic optical-to-electrical conversion dynamics in a graphene photodetector. *Nat. Photonics* **2022**, *16*, 718–723. [[CrossRef](#)]
- Wang, S.B.; Hsiao, C.H.; Chang, S.J.; Lam, K.T.; Wen, K.H.; Hung, S.C.; Young, S.-J.; Huang, B.R. A CuO nanowire infrared photodetector. *Sens. Actuators A Phys.* **2011**, *171*, 207–211. [[CrossRef](#)]
- Bai, Z.; Zhang, Y. Self-powered UV–visible photodetectors based on ZnO/Cu<sub>2</sub>O nanowire/electrolyte heterojunctions. *J. Alloys Compd.* **2016**, *675*, 325–330. [[CrossRef](#)]
- Kumar, K.D.A.; Mele, P.; Golovynskiy, S.; Khan, A.; El-Toni, A.M.; Ansari, A.A.; Gupta, R.K.; Ghaithan, H.; AlFaify, S.; Murahari, P. Insight into Al doping effect on photodetector performance of CdS and CdS:Mg films prepared by self-controlled nebulizer spray technique. *J. Alloys Compd.* **2021**, *892*, 160801. [[CrossRef](#)]
- Shuai, M.; Lingmin, Y.; Lei, C.; Chun, L.; Mingli, Y.; Xinhui, F. Resistive-type UV–visible photodetector based on CdS NWs /ZnO nanowalls heterostructure fabricated using in-situ synthesis method. *J. Alloys Compd.* **2020**, *827*, 154090. [[CrossRef](#)]
- Feng, M.; Lu, W.; Zhou, Y.; Zhen, R.; He, H.; Wang, Y.; Li, C. Synthesis of polypyrrole/nitrogen-doped porous carbon matrix composite as the electrode material for supercapacitors. *Sci. Rep.* **2020**, *10*, 15370. [[CrossRef](#)]
- El Nady, J.; Shokry, A.; Khalil, M.; Ebrahim, S.; Elshaer, A.M.; Anas, M. One-step electrodeposition of a polypyrrole/NiO nanocomposite as a supercapacitor electrode. *Sci. Rep.* **2022**, *12*, 3611. [[CrossRef](#)]
- Hadia, N.M.A.; Eid, S.; Shaban, M.; Mohamed, S.H.; Elsayed, A.M.; Ahmed, A.M.; Alzaid, M.; Abdelazeez, A.A.A.; El Malti, W.; Rabia, M. Poly-3-Methyl Aniline-Assisted Spherical PbS Quantum Dots through the Ionic Adsorption Deposition Method as a Novel and Highly Efficient Photodetector in UV, Vis, and NIR Regions. *Adsorpt. Sci. Technol.* **2022**, *2022*, 7693472. [[CrossRef](#)]

19. Khalafalla, M.A.H.; Hadia, N.M.A.; Elsayed, A.M.; Alruqi, M.; El Malti, W.; Shaban, M.; Rabia, M. ATO/Polyaniline/PbS Nanocomposite as Highly Efficient Photoelectrode for Hydrogen Production from Wastewater with Theoretical Study for the Water Splitting. *Adsorpt. Sci. Technol.* **2022**, *2022*, 5628032. [[CrossRef](#)]
20. Trabelsi, A.B.G.; Elsayed, A.M.; Alkallas, F.H.; Al-Noaimi, M.; Kusmartsev, F.V.; Rabia, M. A Fractal, Flower Petal-like CuS-CuO/G-C3N4 Nanocomposite for High Efficiency Supercapacitors. *Coatings* **2022**, *12*, 1834. [[CrossRef](#)]
21. Trabelsi, A.B.G.; Essam, D.; Alkallas, F.H.; Ahmed, A.M.; Rabia, M. Petal-like NiS-NiO/G-C3N4 Nanocomposite for High-Performance Symmetric Supercapacitor. *Micromachines* **2022**, *13*, 2134. [[CrossRef](#)]
22. Rabia, M.; Essam, D.; Alkallas, F.H.; Shaban, M.; Elaissi, S.; Trabelsi, A.B.G. Flower-Shaped CoS-Co<sub>2</sub>O<sub>3</sub>/G-C3N4 Nanocomposite for Two-Symmetric-Electrodes Supercapacitor of High Capacitance Efficiency Examined in Basic and Acidic Mediums. *Micromachines* **2022**, *13*, 2234. [[CrossRef](#)] [[PubMed](#)]
23. Hien, H.T.; Trung, B.H. Fabrication and research of characteristics of NIO/PPY hybrid films used for NH<sub>3</sub> gas sensor at room temperature. *UTEHY J. Sci. Technol.* **2021**, *31*, 14–20.
24. Zaki, S.E.; Basyooni, M.A.; Shaban, M.; Rabia, M.; Eker, Y.R.; Attia, G.F.; Yilmaz, M.; Ahmed, A.M. Role of oxygen vacancies in vanadium oxide and oxygen functional groups in graphene oxide for room temperature CO<sub>2</sub> gas sensors. *Sens. Actuators A Phys.* **2019**, *294*, 17–24. [[CrossRef](#)]
25. Ahmed, A.M.; Rabia, M.; Shaban, M. The structure and photoelectrochemical activity of Cr-doped PbS thin films grown by chemical bath deposition. *RSC Adv.* **2020**, *10*, 14458–14470. [[CrossRef](#)] [[PubMed](#)]
26. Mohamed, H.S.; Rabia, M.; Zhou, X.-G.; Qin, X.-S.; Khabiri, G.; Shaban, M.; Younus, H.A.; Taha, S.; Hu, Z.-Y.; Liu, J.; et al. Phase-junction Ag/TiO<sub>2</sub> nanocomposite as photocathode for H<sub>2</sub> generation. *J. Mater. Sci. Technol.* **2021**, *83*, 179–187. [[CrossRef](#)]
27. Rabia, M.; Mohamed, S.H.; Zhao, H.; Shaban, M.; Lei, Y.; Ahmed, A.M. TiO<sub>2</sub>/TiO<sub>x</sub>NY Hollow Mushrooms-like Nanocomposite Photoanode for Hydrogen Electrogenation. *J. Porous Mater.* **2020**, *27*, 133–139; Erratum in *J. Porous Mater.* **2020**, *27*, 329. [[CrossRef](#)]
28. Elsayed, A.M.; Rabia, M.; Shaban, M.; Aly, A.H.; Ahmed, A.M. Preparation of Hexagonal Nanoporous Al<sub>2</sub>O<sub>3</sub>/TiO<sub>2</sub>/TiN as a Novel Photodetector with High Efficiency. *Sci. Rep.* **2021**, *11*, 17572. [[CrossRef](#)]
29. Liu, Z.; Li, F.; Li, S.; Hu, C.; Wang, W.; Wang, F.; Lin, F.; Wang, H. Fabrication of UV Photodetector on TiO<sub>2</sub>/Diamond Film. *Sci. Rep.* **2015**, *5*, 14420. [[CrossRef](#)] [[PubMed](#)]
30. Mohamed, F.; Rabia, M.; Shaban, M. Synthesis and characterization of biogenic iron oxides of different nanomorphologies from pomegranate peels for efficient solar hydrogen production. *J. Mater. Res. Technol.* **2020**, *9*, 4255–4271. [[CrossRef](#)]
31. Hadia, N.M.A.; Abdelazez, A.A.A.; Alzaid, M.; Shaban, M.; Mohamed, S.H.; Hoex, B.; Hajjiah, A.; Rabia, M. Converting Sewage Water into H<sub>2</sub> Fuel Gas Using Cu/CuO Nanoporous Photocatalytic Electrodes. *Materials* **2022**, *15*, 1489. [[CrossRef](#)] [[PubMed](#)]
32. Kunwar, S.; Pandit, S.; Jeong, J.-H.; Lee, J. Improved Photoresponse of UV Photodetectors by the Incorporation of Plasmonic Nanoparticles on GaN Through the Resonant Coupling of Localized Surface Plasmon Resonance. *Nano-Micro Lett.* **2020**, *12*, 91. [[CrossRef](#)] [[PubMed](#)]
33. Luo, S.; Yu, Y.; Cheng, N.; Qi, X.; Luo, S.; Liu, Y.; Zhong, J. Solution-processed GeSe/CdS heterogenous film for self-powered photodetectors. *Ceram. Int.* **2023**, *49*, 11302–11310. [[CrossRef](#)]
34. Ravikumar, A.P.; Garcia, T.A.; De Jesus, J.; Tamargo, M.C.; Gmachl, C.F. High detectivity short-wavelength II-VI quantum cascade detector. *Appl. Phys. Lett.* **2014**, *105*, 061113. [[CrossRef](#)]
35. Chen, H.; Yu, P.; Zhang, Z.; Teng, F.; Zheng, L.; Hu, K.; Fang, X. Ultrasensitive Self-Powered Solar-Blind Deep-Ultraviolet Photodetector Based on All-Solid-State Polyaniline/MgZnO Bilayer. *Small* **2016**, *12*, 5809–5816. [[CrossRef](#)]
36. Kalra, A.; Vura, S.; Rathkanthiwar, S.; Muralidharan, R.; Raghavan, S.; Nath, D.N. Demonstration of high-responsivity epitaxial β-Ga<sub>2</sub>O<sub>3</sub>/GaN metal-heterojunction-metal broadband UV-A/UV-C detector. *Appl. Phys. Express* **2018**, *11*, 064101. [[CrossRef](#)]
37. Costas, A.; Florica, C.; Preda, N.; Apostol, N.; Kuncser, A.; Nitescu, A.; Enculescu, I. Radial heterojunction based on single ZnO-CuxO core-shell nanowire for photodetector applications. *Sci. Rep.* **2019**, *9*, 5553. [[CrossRef](#)]
38. Hong, Q.; Cao, Y.; Xu, J.; Lu, H.; He, J.; Sun, J.-L. Self-Powered Ultrafast Broadband Photodetector Based on p-n Heterojunctions of CuO/Si Nanowire Array. *ACS Appl. Mater. Interfaces* **2014**, *6*, 20887–20894. [[CrossRef](#)]
39. Tan, W.-C.; Shih, W.-H.; Chen, Y.F. A Highly Sensitive Graphene-Organic Hybrid Photodetector with a Piezoelectric Substrate. *Adv. Funct. Mater.* **2014**, *24*, 6818–6825. [[CrossRef](#)]
40. Lan, T.; Fallatah, A.; Suiter, E.; Padalkar, S. Size Controlled Copper (I) Oxide Nanoparticles Influence Sensitivity of Glucose Biosensor. *Sensors* **2017**, *17*, 1944. [[CrossRef](#)]
41. Liu, K.; Sakurai, M.; Liao, M.; Aono, M. Giant Improvement of the Performance of ZnO Nanowire Photodetectors by Au Nanoparticles. *J. Phys. Chem. C* **2010**, *114*, 19835–19839. [[CrossRef](#)]
42. Liu, Y.; Guo, P.; Gao, P.; Tong, J.; Li, J.; Wang, E.; Wang, C.; Xia, Y. Effect of fluorine atoms on optoelectronic, aggregation and dielectric constants of 2,1,3-benzothiadiazole-based alternating conjugated polymers. *Dye. Pigment.* **2021**, *193*, 109486. [[CrossRef](#)]
43. Tian, J.; Xue, Q.; Yao, Q.; Li, N.; Brabec, C.J.; Yip, H. Inorganic Halide Perovskite Solar Cells: Progress and Challenges. *Adv. Energy Mater.* **2020**, *10*, 2000183. [[CrossRef](#)]
44. Zheng, L.; Teng, F.; Zhang, Z.; Zhao, B.; Fang, X. Large scale, highly efficient and self-powered UV photodetectors enabled by all-solid-state n-TiO<sub>2</sub> nanowell/p-NiO mesoporous nanosheet heterojunctions. *J. Mater. Chem. C* **2016**, *4*, 10032–10039. [[CrossRef](#)]

45. Naldoni, A.; Guler, U.; Wang, Z.; Marelli, M.; Malara, F.; Meng, X.; Besteiro, L.V.; Govorov, A.O.; Kildishev, A.V.; Boltasseva, A.; et al. Broadband Hot-Electron Collection for Solar Water Splitting with Plasmonic Titanium Nitride. *Adv. Opt. Mater.* **2017**, *5*, 1601031. [[CrossRef](#)]
46. Zheng, L.; Hu, K.; Teng, F.; Fang, X. Novel UV-Visible Photodetector in Photovoltaic Mode with Fast Response and Ultrahigh Photosensitivity Employing Se/TiO<sub>2</sub> Nanotubes Heterojunction. *Small* **2017**, *13*, 1602448. [[CrossRef](#)]
47. Zheng, L.; Yu, P.; Hu, K.; Teng, F.; Chen, H.; Fang, X. Scalable-Production, Self-Powered TiO<sub>2</sub> Nanowell–Organic Hybrid UV Photodetectors with Tunable Performances. *ACS Appl. Mater. Interfaces* **2016**, *8*, 33924–33932. [[CrossRef](#)]

**Disclaimer/Publisher’s Note:** The statements, opinions and data contained in all publications are solely those of the individual author(s) and contributor(s) and not of MDPI and/or the editor(s). MDPI and/or the editor(s) disclaim responsibility for any injury to people or property resulting from any ideas, methods, instructions or products referred to in the content.